The Cytoskeleton Maintains Organelle Partitioning Required for Single-Cell C$_4$ Photosynthesis in Chenopodiaceae Species [W]

Simon D.X. Chuong,[1] Vincent R. Franceschi, and Gerald E. Edwards

School of Biological Sciences, Washington State University, Pullman, Washington 99164-4236

Recently, three Chenopodiaceae species, *Bienertia cycloptera*, *Bienertia sinuspersici*, and *Suaeda aralocaspica*, were shown to possess novel C$_4$ photosynthesis mechanisms through the compartmentalization of organelles and photosynthetic enzymes into two distinct regions within a single chlorenchyma cell. *Bienertia* has peripheral and central compartments, whereas *S. aralocaspica* has distal and proximal compartments. This compartmentalization achieves the equivalent of spatial separation of Kranz anatomy, including dimorphic chloroplasts, but within a single cell. To characterize the mechanisms of organelle compartmentalization, the distribution of the major organelles relative to the cytoskeleton was examined. Examination of the distribution of the cytoskeleton using immunofluorescence studies and transient expression of green fluorescent protein–tagged cytoskeleton markers revealed a highly organized network of actin filaments and microtubules associating with the chloroplasts and showed that the two compartments in each cell had different cytoskeletal arrangements. Experiments using cytoskeleton-disrupting drugs showed in *Bienertia* and *S. aralocaspica* that microtubules are critical for the polarized positioning of chloroplasts and other organelles. Compartmentalization of the organelles in these species represents a unique system in higher plants and illustrates the degree of control the plant cell has over the organization and integration of multiorganellar processes within its cytoplasm.

INTRODUCTION

In terrestrial plants, three basic types of photosynthetic mechanisms, C$_3$, C$_4$, and Crassulacean acid metabolism, have been identified, and each is associated with distinct anatomies (Edwards and Walker, 1983; Winter and Smith, 1996; Sage, 1999; Edwards et al., 2001a, 2001b). C$_4$ plants have a CO$_2$-concentrating mechanism and have classically been recognized as having Kranz anatomy, which consists of two biochemically and ultrastructurally distinct photosynthetic cell types that function cooperatively to fix atmospheric CO$_2$ (Hatch and Slack, 1970; Hatch et al., 1971; Edwards and Huber, 1981). One cell type, mesophyll cells, fix atmospheric carbon via phosphoenolpyruvate carboxylase (PEPC), and the C$_4$ product is transported to the other cell type, bundle sheath cells, which decarboxylate this product and refix the released CO$_2$ via ribulose-1,5-bisphosphate carboxylase/oxygenase (Rubisco). The end result is an increase in CO$_2$ concentration relative to O$_2$ around the chloroplasts, which depresses photorespiration and gives rise to the greater efficiency of C$_4$ plants under certain conditions. Therefore, C$_4$ plants often exhibit significantly higher water use efficiency, greater tolerance to high temperature, and higher photosynthetic rates compared with C$_3$ plants (Hatch, 1971;

Edwards and Huber, 1981; Sage, 2005). Given these features, there has been much interest in the potential for engineering C$_4$ photosynthesis into C$_3$ plants (Ku et al., 1999; Sheehy et al., 2000; Edwards et al., 2001a; Matsuoka et al., 2001; Leegood, 2002), but the prospect of complex anatomical modification as well as the targeted expression of a number of enzymes make this a particularly challenging task.

It has long been accepted that the cellular separation of biochemical functions in Kranz anatomy is required for the C$_4$ cycle to operate in terrestrial plants; recently, however, this paradigm has been broken with the discoveries of three species in the family Chenopodiaceae that are capable of performing the entire C$_4$ photosynthesis cycle in individual chlorenchyma cells of the leaf (Freitag and Stichler, 2000; Voznesenskaya et al., 2001, 2002; Freitag and Stichler, 2002; Edwards et al., 2004; Akhani et al., 2005) These discoveries have led to a reexamination of the requirements for C$_4$ photosynthesis and raise interesting questions about the evolution of the syndrome as well as the potential for engineering C$_4$ photosynthesis into C$_3$ crop plants without having to generate the dual cell system. In addition, they provide exquisite examples of the ability of plant cells to generate and maintain biochemically complex compartments based on both the partitioning of organelles and the differential regulation of gene expression in these organelles within the same cell.

Single-cell C$_4$ photosynthesis has been found in *Bienertia cycloptera* (Voznesenskaya et al., 2002), *Bienertia sinuspersici* (Akhani et al., 2005; Voznesenskaya et al., 2005), and *Suaeda aralocaspica* (Voznesenskaya et al., 2001). *S. aralocaspica* was originally called *Borszczowia aralocaspica*. However, recent molecular phylogenetic studies classified *B. aralocaspica* in the genus *Suaeda* (Schütze et al., 2003; Kapralov et al., 2006).

Biochemical analysis of photosynthetic enzymes, carbon isotope discrimination analysis, and measurement of gas-exchange parameters demonstrated that all three species conduct full C_4 photosynthesis under normal growth conditions. Furthermore, studies showed that this amazing feature of C_4 photosynthesis in a single chlorenchyma cell is partly accomplished by the partitioning of two biochemically and ultrastructurally distinct chloroplast types into separate compartments within the cell (Voznesenskaya et al., 2001, 2002, 2005). The chlorenchyma cells of the two *Bienertia* species have a peripheral chloroplast-containing cytoplasmic compartment (PCC) and a central cytoplasmic compartment (CCC) proposed to function like mesophyll and bundle sheath cells, respectively, in analogy to Kranz type C_4. Surprisingly, a completely different solution to performing C_4 photosynthesis in a single cell is found in *Suaeda aralocaspica*. This species produces elongated palisade chlorenchyma cells with dimorphic chloroplasts polarized toward opposite ends of the cell. This is somewhat analogous to having Kranz anatomy, with the mesophyll and bundle sheath arrangement, but without the intervening cell walls. In both systems, the partitioning of biochemically distinct organelles into discrete compartments is believed to result in the concentration of CO_2 around the Rubisco-containing chloroplasts, causing the inhibition of Rubisco oxygenase activity and photorespiration, as occurs in the typical Kranz system (Edwards et al., 2004). Models of how these systems operate C_4 photosynthesis have been proposed (Edwards et al., 2004); however, much work remains to characterize the cell biology of these recently discovered, unusual cells.

To further our understanding of these systems, a question that needs to be answered concerns the basic nature of the mechanism to maintain the positioning of the organelles in the two compartments of the cells, because loss of this partitioning would make it impossible for the C_4 cycle to operate properly. A likely cellular component in the establishment and maintenance of organelle compartmentalization in these unique cells is the cytoskeleton. In plants, it participates in numerous important developmental processes, such as cell division, cell elongation, cell signaling, and organelle movement and positioning (Staiger and Lloyd, 1994; Wasteneys and Yang, 2004). Evidence for a role of the cytoskeleton in organelle movements has been shown in various eukaryotic cells. Microtubule-based motility has been shown to be involved in organelle movement and vesicle transport in animal cells (Kuznetsov et al., 1992; Rogers and Gelfand, 1998, 2000), whereas organelle movement in plants involved an actin filament–based system (Williamson, 1993). In plant cells, the actin cytoskeleton has been shown to be involved in the movement of chloroplasts (Kandasamy and Meagher, 1999), the endoplasmic reticulum (ER) (Boevink et al., 1998), the Golgi apparatus (Boevink et al., 1998; Nebenfuhr et al., 1999), mitochondria (Van Gestel et al., 2002), nuclei (Chytilova et al., 2000; Sliwinska et al., 2002), and peroxisomes (Collings et al., 2002; Jedd and Chua, 2002; Mano et al., 2002; Mathur et al., 2002). However, recent studies demonstrated the involvement of microtubules in the positioning of mitochondria (Van Gestel et al., 2002), nuclei (Chytilova et al., 2000) and peroxisome dynamics (Chuong et al., 2005), and the movement of chloroplasts and vesicles during cytokinesis (Sheahan et al., 2004), suggesting that both elements of the cytoskeleton may function coopera-

tively during organelle movement and organization. The purpose of this study was to examine the role of components of the cytoskeleton in maintaining the partitioning of dimorphic chloroplasts as well as mitochondria and peroxisomes in chlorenchyma cells of *B. sinuspersici* and *S. aralocaspica*. Polarization of organelles between two major cellular compartments was observed, and the significance of organelle compartmentalization and the role of the cytoskeleton in the anchoring and maintenance of these separate compartments are discussed. The results provide important insights into the cell biology of these remarkable single-cell C_4 systems and, in general, are relevant to elucidating the mechanisms of cellular polarization in plant cells.

RESULTS

General Chlorenchyma Cell Anatomy and Enzyme Localization

Casual observation of the anatomy of the leaves of both species revealed a very unusual polarization or compartmentalization of the chlorenchyma cell cytoplasm. In mature leaves of *Bienertia*, the chlorenchyma consists of two to three layers of semicylindrical cells with extensive intercellular spaces between them (Figure 1A). These cells have a thin PCC that is connected to a large, spherical CCC by transvacuolar cytoplasmic channels along the medial transverse plane of the cell (Figure 1A, small arrows). The CCC has been shown to contain numerous chloroplasts with well-developed grana, whereas chloroplasts with a lower granal index are distributed along the thin PCC (Voznesenskaya et al., 2002). In mature *S. aralocaspica* leaves, the chlorenchyma occurs as a single layer of elongate cylindrical cells tightly packed together (Figure 1B). *S. aralocaspica* chlorenchyma cells have a dense layer of chloroplasts in the proximal region of the cell, which is oriented toward the center of the leaf and adjacent to the vascular tissues. There are fewer chloroplasts located along the periphery of the distal end of the cell, which is oriented toward the epidermis or leaf surface, where CO_2 enters. These chloroplasts are deficient in grana, whereas grana-type chloroplasts are concentrated in the proximal end of the cells (Voznesenskaya et al., 2001).

Immunolocalization of major photosynthetic enzymes indicated that the partitioning of cytoplasm seen in both species is related to the mechanism of C_4 photosynthesis in single cells. Antibodies to Rubisco, which in Kranz anatomy is associated with the bundle sheath, gave specific and intensive labeling in the CCC but not in the PCC of *Bienertia* chlorenchyma cells (Figure 1C) and in the proximal end but not in the distal end of *S. aralocaspica* chlorenchyma cells (Figure 1D). By contrast, labeling for pyruvate orthophosphate dikinase (PPDK), a C_4-specific enzyme located in mesophyll cells of Kranz anatomy C_4 systems, was predominantly in peripheral regions of *Bienertia* and distal regions of the *S. aralocaspica* cells, with weak labeling in the central regions of *Bienertia* and proximal compartments of *S. aralocaspica* (Figures 1E and 1F). The localization of another key enzyme in photosynthetic CO_2 fixation for the C_4 pathway, NADP–malate dehydrogenase (NADP-MDH), was localized predominantly to chloroplasts of the peripheral and distal compartments, with low labeling in the central and proximal
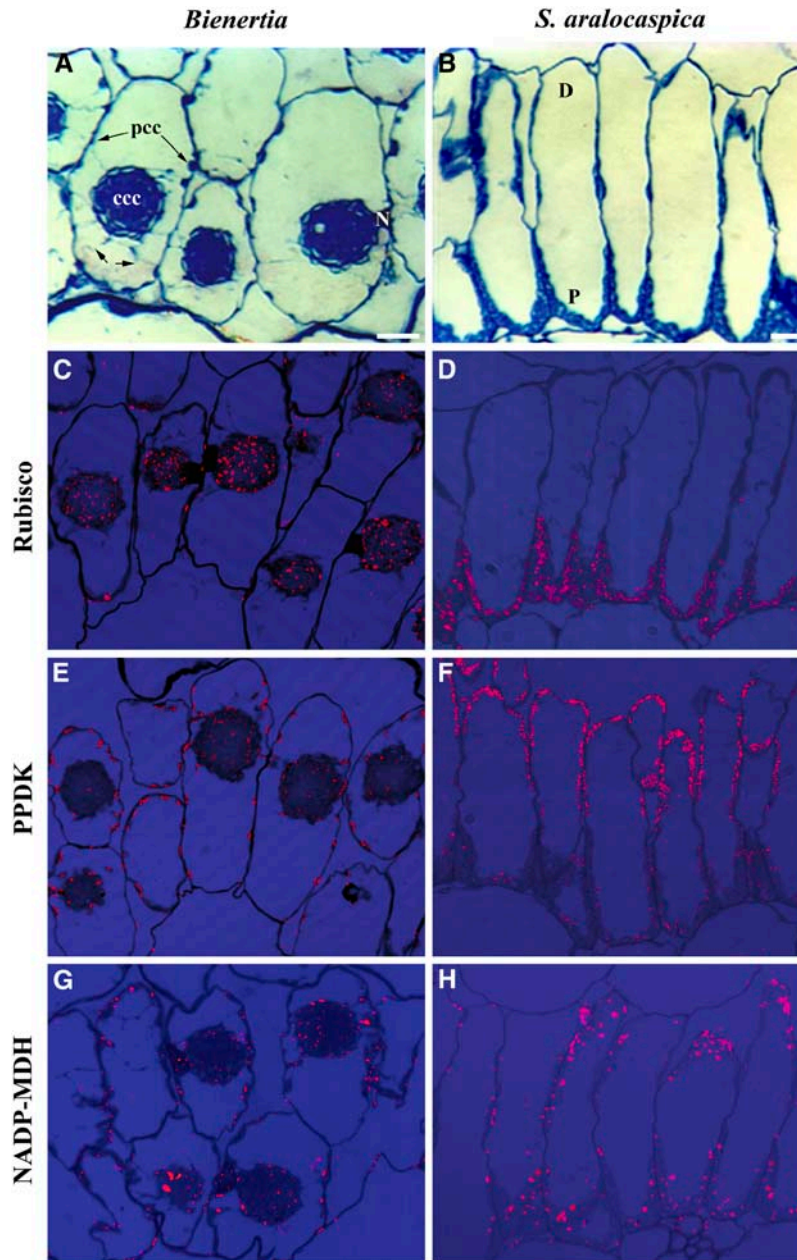
Figure 1. General *B. sinuspersici* and *S. aralocaspica* Chlorenchyma Cell Anatomy and in Situ Immunolocalization of Rubisco, PPDK, and NADP-MDH.

(A) Cross section of a *Bienertia* leaf showing a chlorenchyma cell containing two cytoplasmic compartments, a CCC and a PCC. Cytoplasmic channels connect the two compartments (small arrows).
(B) Cross section of an *S. aralocaspica* leaf showing chlorenchyma cells with organelles compartmentalized in the distal (D) and proximal (P) regions.
(C) In *Bienertia*, Rubisco is localized mainly in the chloroplasts of the CCC.
(D) In *S. aralocaspica*, Rubisco is localized in the chloroplasts of the proximal compartment.
(E) In *Bienertia*, PPDK is highly concentrated in the chloroplasts in the PCC, with lower levels in the CCC.
(F) In *S. aralocaspica*, PPDK is strongly localized to chloroplasts in the distal compartment.
(G) In *Bienertia*, NADP-MDH is localized mainly in the chloroplasts of the peripheral compartment.
(H) In *S. aralocaspica*, NADP-MDH is localized mainly in the chloroplasts of the distal compartment.
N, nucleus. Bars = 20 μm.

compartments, respectively, in both single-cell C_4 species (Figures 1G and 1H). Protein gel blot analysis, shown in Figure 2, comparing these species with a related Kranz anatomy C_4 species (*Suaeda eltonica*) and a C_3 species (*Suaeda heterophylla*) confirmed that both *Bienertia* species and *S. aralocaspica* have the major enzymes associated with C_4 photosynthesis. The weak immunoreactive bands observed for PEPC and NAD–malic enzyme (NAD-ME) in the C_3 species most likely represent isoforms of the enzymes that are constitutively expressed in C_3 plants.

Organelles Are Partitioned to Distinct Cellular Compartments

The differential distribution of two types of chloroplasts demonstrated previously within the chlorenchyma cells of these two species suggested that other organelles may be nonrandomly distributed as well. The distribution of organelles in *Bienertia* and *S. aralocaspica* chlorenchyma cells was observed using various cell-permeant fluorescent probes that selectively associate with specific organelles in live cells. In mature *Bienertia* chlorenchyma cells, chlorophyll autofluorescence imaging clearly demonstrated the distribution of chloroplasts in the peripheral and central cytoplasmic regions (Figure 3). The 3,3′-dihexyloxacarbocyanine iodide [DiOC$_6$(3)], which partitions into the ER, showed that in both species the reticulated tubular ER is enriched in the compartment having the PPDK-containing chloroplasts, although some ER was also evident in the region of the more densely packed Rubisco-containing chloroplasts (Figures 3A and 3F). Rhodamine 123, which selectively partitions into mitochondria, showed that the majority of mitochondria in *Bienertia* were concentrated in the CCC, although a few mitochondria were occasionally observed in the PCC (Figure 3B), whereas in *S. aralocaspica*, essentially all of the mitochondria were at the proximal end of the cell (Figure 3G). Nuclei were
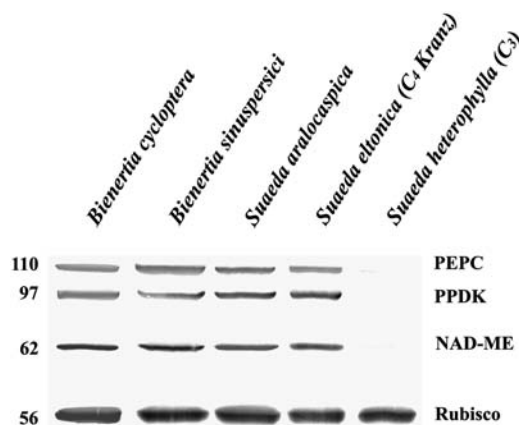
visualized in cells stained with acridine orange and were found to be in a very specific location in almost all cells examined. In *Bienertia*, they were located between the PCC and the CCC (Figure 3C), whereas in *S. aralocaspica*, they were at the interface between the densely packed chloroplasts of the proximal end and those of the distal compartment (Figure 3H).

Because a good live cell probe was not available for peroxisomes, we used an antibody raised against the peroxisomal matrix enzyme catalase to show their intracellular localization with respect to chloroplasts. Immunofluorescence studies showed that most of the peroxisomes were concentrated in the CCC of *Bienertia* (Figure 3D) and in the proximal end of *S. aralocaspica* cells (Figure 3I), although some peroxisomes were also observed in the peripheral and distal compartments of *Bienertia* and *S. aralocaspica* cells, respectively. Nevertheless, in both cell types they were typically associated with chloroplasts. This observation is consistent with the transient expression of a green fluorescent protein–peroxisomal matrix protein (GFP-MFP) that demonstrated that some peroxisomes are mobile within the chlorenchyma cells of *Bienertia* (Figure 4). GFP-MFP–transformed cells showed punctate structures that are presumed to be peroxisomes throughout the cell. Most peroxisomes were stationary, displaying only oscillatory motions (Figure 4, stars), whereas some peroxisomes exhibited directional movements at velocities up to 2 μm/s (Figure 4, arrows and arrowheads). Cells exposed to carboxy-DCFDA, which partitions into vacuoles, showed that the vacuole in *Bienertia* is actually one large, interconnected compartment, although in a single median optical slice it may appear to be separated into two compartments by the CCC (Figure 3E). The *S. aralocaspica* vacuole was one large compartment with no transvacuolar cytoplasmic strands (Figure 3J).

Chloroplasts Interact with Cytoskeletal Elements

Because the unusual partitioning of organelles in both species is critical to the function of C_4 in a single cell, it is important to understand how it is maintained. A likely cellular component that functions in this partitioning is the cytoskeleton. We conducted a number of experiments to test this notion.

Scanning electron microscopy imaging of cryofractured and detergent-etched cells indicated a resistant network of cables associated with the chloroplasts of both species (see Supplemental Figure 1 online, arrowheads). In *Bienertia*, the resistant network appeared to be associated primarily with the peripheral chloroplasts and the chloroplasts in the outer region of the CCC (see Supplemental Figures 1A to 1C online, arrowheads). In *S. aralocaspica*, this network appeared to be most extensive in the cytoplasm of the distal portion of the cell and was clearly associated with chloroplasts in this region (see Supplemental Figures 1D to 1G online, arrowheads). Immunofluorescence studies of intact cells were then performed for the localization of actin filaments and microtubules to confirm the nature of this network.

Screening of the antisera used by protein gel blot analysis indicated that these monoclonal antibodies reacted strongly and specifically with a 42-kD actin band and a 50-kD tubulin band in total protein extracts of both *Bienertia* and *S. aralocaspica* (see

Figure 2. *B. sinuspersici* and *S. aralocaspica* Belong to the NAD-ME Group of C_4 Plants.

Immunoblot showing the reactivity of *Bienertia* and *S. aralocaspica* total proteins to C_4 enzymes and Rubisco. Protein blots were probed with polyclonal antibodies raised against *Z. mays* PEPC and PPDK, *Amaranthus hydrochondriacus* NAD-ME, and *Spinacia oleracea* Rubisco large subunit. Numbers at left indicate molecular mass standards in kilodaltons.
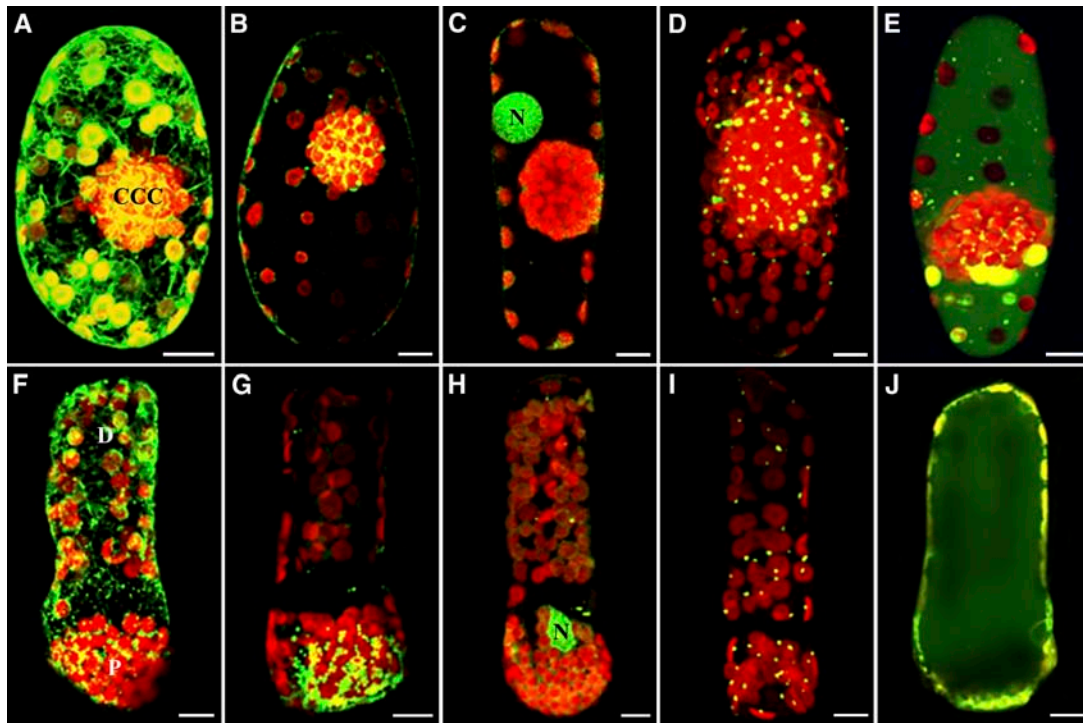
Figure 3. Cell-Permeant Fluorescent Staining and Immunofluorescence Labeling Showing the Distribution of ER, Mitochondria, Nuclei, Peroxisomes, and Vacuoles in *B. sinuspersici* and *S. aralocaspica* Chlorenchyma Cells.

Representative results from three separate experiments are shown. Confocal microscopy of live and fixed *Bienertia* (**[A]** to **[E]**) and *S. aralocaspica* (**[F]** to **[J]**) chlorenchyma cells stained with various organelle-specific fluorescent dyes and antibodies demonstrate their spatial relationship with chloroplasts (red). Bars = 10 μm.

(A) and **(F)** Projections of chlorenchyma cells stained with DiOC$_6$(3) showing reticular structures (green).

(B) and **(G)** Projections of rhodamine 123–stained chlorenchyma cells showing the concentration of mitochondria (yellow-green) in the CCC and proximal compartment.

(C) and **(H)** Single optical section **(C)** and projection of acridine orange–stained cells **(H)** showing the prominent position of nuclei (N; green) relative to the CCC and proximal compartment.

(D) and **(I)** Projections of fixed cells probed with catalase and Oregon green–conjugated secondary antibodies to visualize peroxisome (yellow-green) distribution.

(E) and **(J)** Single optical sections through the midplane of 5′(6)-carboxy-2′7′-dichlorofluorescein diacetate (carboxy-DCFDA)–stained cells showing the large vacuoles (green).

Supplemental Figure 2 online). Based on their specificities, we then used these antibodies to stain actin filaments and microtubules in whole *Bienertia* and *S. aralocaspica* chlorenchyma cells for our microscopy investigations. For the images presented, the cytoskeleton and chloroplasts were colocalized, as observed by fluorescence emission of cytoskeleton bound to Oregon green–conjugated secondary antibodies at 488 nm and imaging of the autofluorescence of chlorophyll at 568 nm.

The immunofluorescence experiments with actin antibody revealed two types of actin filaments in *Bienertia* and *S. aralocaspica* chlorenchyma cells: an extensive array of actin filament bundles and a network of fine actin filaments. In *Bienertia*, the thick actin filament bundles emanated from the CCC and extended primarily into the radial peripheral cytoplasm (Figures 5A and 5E), whereas in *S. aralocaspica*, extensive longitudinal arrays of actin bundles from the distal region of the cell extended into the proximal compartment, interweaving among the densely packed chloroplasts (Figures 5G and 5H). Finer actin filaments

that derived from the bundles extended into the cell cortex and were often associated with chloroplasts (Figure 5H). Actin cables attached directly to the nucleus or nuclear basket were also observed (Figures 5A, 5E to 5H, and 5K). Generally, it was observed that most chloroplasts were associated directly with actin filaments, and baskets of thin actin filaments were often seen surrounding individual chloroplasts (Figures 5B to 5D). In *S. aralocaspica* chlorenchyma cells, chloroplasts in the distal compartment were aligned along the longitudinally arranged, thick actin bundles and attached to fine actin filaments originating from these cables (Figures 5G to 5J). In both species, most of the chloroplasts observed were completely or partially surrounded by actin filaments forming basket-like or ring-like structures (Figures 5C, 5D, 5L, and 5M).

Immunofluorescence studies with anti–β-tubulin antibody revealed similar extensive arrays of microtubules but with somewhat different orientations. In *Bienertia* cells, dense arrays of microtubules were observed surrounding the CCC, whereas
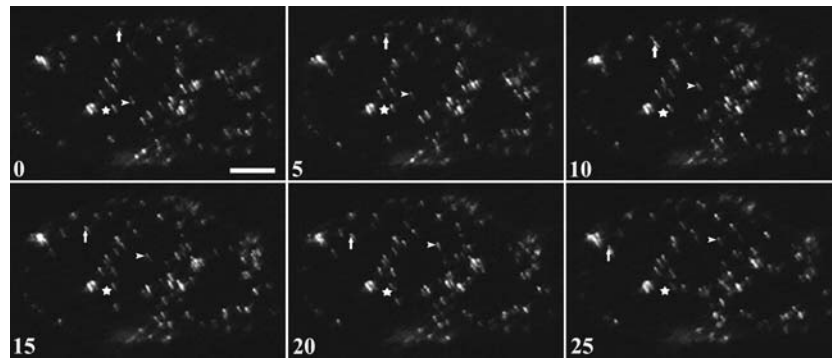
Figure 4. Peroxisomal Motility in *B. sinuspersici* Chlorenchyma Cells Transiently Expressing GFP-MFP.

Time-lapse images of a GFP-MFP–expressing *B. sinuspersici* chlorenchyma cell. The movement of three peroxisomes was monitored for 25 s. One of these peroxisomes (stars) showed oscillatory movement over the entire series. Another peroxisome (arrowheads) remained fixed at a site for 5 s and then exhibited short-distance movement during the last 20 s. A third peroxisome (arrows) demonstrated continuous movement through the cytosol, covering a total distance of >40 μm. Numbers indicate elapsed time in seconds. Bar = 15 μm.

intricate networks of microtubules were also observed in the peripheral cytoplasm of the cell (Figures 6A and 6B). The microtubules in the peripheral compartment had a clear association with chloroplasts, often outlining them (Figures 6C and 6D). The CCC appeared to be surrounded by a particularly thick microtubular cage (Figure 6E) compared with a finer microtubular cage surrounding the nucleus (Figure 6F). In *S. aralocaspica*, in contrast with the strong longitudinal orientation of actin bundles, the extensive arrays of microtubules demonstrated a predominantly transverse or oblique orientation in the peripheral cytoplasm (Figures 6G and 6H). There was also a close structural interaction between microtubules and chloroplasts in *S. aralocaspica*, as confocal images of optical sections of these cells showed that many microtubules were present in the same plane as the chloroplasts (Figures 6I to 6K). In fact, in both species, microtubules appeared as vertices that seemingly tethered the chloroplasts in position or completely wrapped around them (Figures 6D and 6K). Similar to *Bienertia*, microtubules in *S. aralocaspica* were also observed surrounding the nucleus (Figures 6F, 6L, and 6M).

Immunofluorescence studies were also performed on chlorenchyma cells of *S. heterophylla* (C₃) and *S. eltonica* (C₄ Kranz) plants to illustrate the organization of actin filaments and microtubules (see Supplemental Figure 3 online). Extensive cytoskeletal networks were observed in mesophyll cells of both species as well as in bundle sheath cells of *S. eltonica*, and these networks appeared to have close interaction with chloroplasts (see Supplemental Figures 3C and 3D and insets in Figures 3E to 3H online). To determine whether the intimate interactions of cytoskeletal components with chloroplasts are authentic and not a result of chemically induced artifacts, transient transformation of *Bienertia* chlorenchyma cells with cytoskeleton binding proteins fused to GFP was performed. In cells that transiently expressed GFP-talin, an actin binding protein, similar thick microfilament bundles were observed emanating from the nucleus positioned near the central compartment (Figure 7A). Finer actin filaments were also observed to interact with chloroplasts in the cortical region (Figure 7B). Similarly, in *Bienertia* cells

transformed with GFP-MAP4, a microtubule-associated protein, a more extensive microtubule network was observed in the cortical region (Figure 7C). Furthermore, an optical section of the cortical region revealed microtubules in the same plane as chloroplasts (Figure 7C, inset).

Organelle Partitioning in *Bienertia* and *S. aralocaspica* Is Dependent on Microtubules

Given the robust actin and microtubule cytoskeletal networks described above, the question arises whether one or both elements are responsible for maintaining the organization of the organelles in the chlorenchyma of *Bienertia* and *S. aralocaspica*. To assess the role of each of the cytoskeleton components in stabilizing organelle partitioning, we analyzed chloroplast distribution in living chlorenchyma cells treated with the cytoskeleton-depolymerizing drugs cytochalasin D (CD), which disrupts actin filaments, and oryzalin (Ory), which disrupts microtubules. Living, isolated *Bienertia* chlorenchyma cells and *S. aralocaspica* leaf sections were used. Within 30 min of treatment of *Bienertia* chlorenchyma cells with Ory, the ball of chloroplasts in the CCC began to disperse, indicating that the integrity of the CCC had been disrupted by the Ory (Figures 8G to 8I). After removal of the drug, treated *Bienertia* chlorenchyma cells were monitored for up to 24 h for cell viability. Ory-treated chlorenchyma cells did not recover, as indicated by the lack of CCC reformation and the absence of fluorescent dye uptake by mitochondria and the endomembrane system (see Supplemental Figures 4C and 4F online). Examination of the cytoskeleton in these treated cells using immunofluorescence demonstrated that the microtubules were completely disrupted but the actin cytoskeleton was still intact (Figure 8H). By contrast, treatment of the cells with the actin filament inhibitor CD (Figures 8D and 8F) did not cause any noticeable changes in the CCC organization compared with controls. The CCC remained intact even after treatment for 2 h or longer (Figures 8D to 8F). These CD-treated cells showed fluorescence staining of both mitochondria and cortical ER that appeared as patches
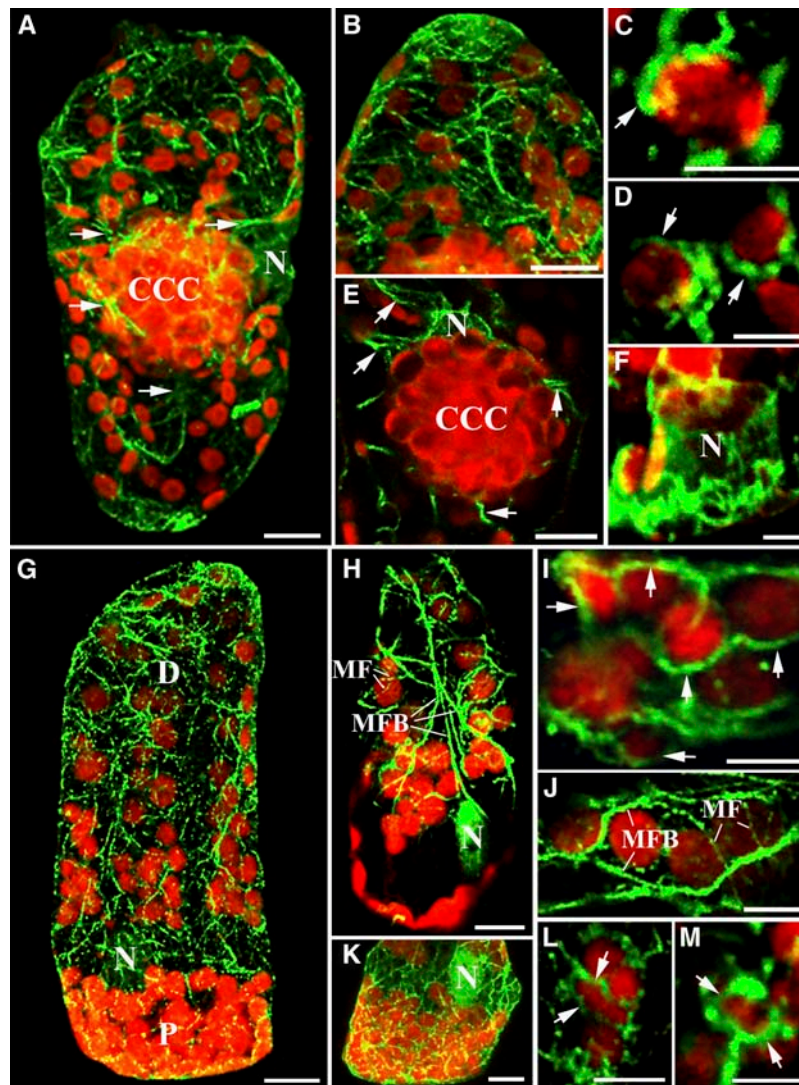
Figure 5. The Actin Cytoskeleton in Chlorenchyma Cells of *B. sinuspersici* and *S. aralocaspica*.

Immunofluorescence staining of actin demonstrates actin–chloroplast association in *Bienertia* and *S. aralocaspica* chlorenchyma cells. Actin filaments (green) were visualized with Oregon green–conjugated secondary antibody, and chloroplasts (red) were observed using their autofluorescence. Except for **(A)**, **(B)**, and **(G)**, the images are single optical sections that demonstrate the direct interaction between actin filaments and chloroplasts. These images represent merged images of the dual channels that show their interaction. This is a representative result from at least five separate experiments with >50 cells observed. Arrows in **(A)** and **(E)** show the thick actin filament bundles connecting the CCC and the PCC. **(G)**, **(H)**, and **(K)** show that the nucleus (N) is also surrounded by actin filaments. Bars = 10 μm in **(A)**, **(B)**, **(E)**, **(G)**, **(H)**, and **(K)** and 5 μm in **(C)**, **(D)**, **(F)**, **(I)**, **(J)**, **(L)**, and **(M)**.
(A) and **(G)** Composite images (projections) of 30 optical 0.8-μm sections depicting the general actin filament patterns in *Bienertia* and *S. aralocaspica* chlorenchyma cells, respectively.
(B) Projection of a low-resolution image of the PCC showing the general distribution of the actin filaments.
(C) and **(D)** Single optical sections of high magnification of a region within the peripheral compartment demonstrating the close contact of actin filaments (arrows) with the chloroplasts.
(E) and **(F)** Single optical sections illustrating actin filaments surrounding and emanating from the nucleus (N).
(G) and **(H)** Projection **(G)** and single optical section **(H)** showing the two types of actin filaments: thick actin microfilament bundles (MFB) and thin actin microfilaments (MF) in *S. aralocaspica*.
(I) and **(J)** Single optical sections demonstrating the positioning of chloroplasts along the actin cables (arrows) by attaching to the thin actin filaments in the distal compartment.
(K) Optical section showing the actin filament pattern in the proximal compartment.
(L) and **(M)** Single optical sections of closeup images showing baskets of actin filaments (arrows) completely surrounding the chloroplasts.
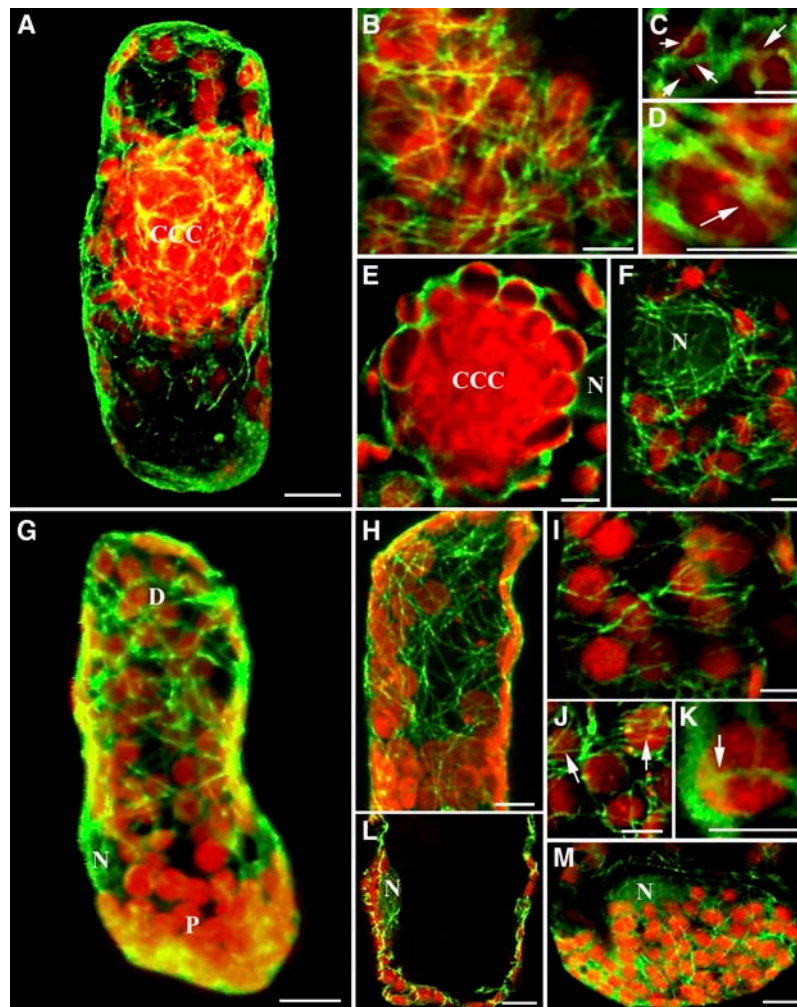
Figure 6. The Microtubule Cytoskeleton in Chlorenchyma Cells of *B. sinuspersici* and *S. aralocaspica*.

Fixed chlorenchyma cells were labeled with anti-tubulin antiserum. Microtubules (green) were visualized with Oregon green–conjugated secondary antibody, the chloroplasts (red) were imaged using their autofluorescence, and the dual-wavelength confocal microscopic images were merged showing their association. This is a representative result obtained from at least five separate experiments with >50 cells observed. Bars = 10 μm in **(A)**, **(G)**, **(L)**, and **(M)** and 5 μm in **(B)** to **(F)** and **(H)** to **(K)**.

(A) and **(G)** Projections of a z-series of 30 optical 0.8-μm sections illustrating the overall microtubule patterns in *Bienertia* and *S. aralocaspica* chlorenchyma cells, respectively.

(B) Single optical section of the cortical region of a chlorenchyma cell to demonstrate an extensive network of microtubules.

(C) and **(D)** Single optical sections of closeup images showing a ring of microtubules (arrows) surrounding the peripheral chloroplasts.

(E) Single optical slice taken at the midpoint of the CCC surrounded by a thick cage of microtubules.

(F) Single optical section image of the cortical region showing microtubules surrounding the nucleus (N).

(H) Projection of the distal compartment showing a dense network of microtubules.

(I) Single optical section of the distal compartment showing transverse or oblique microtubules.

(J) and **(K)** Single optical sections of closeup images of chloroplasts in the distal region surrounded by rings of microtubules. Arrows indicate rings or baskets of microtubules around chloroplasts.

(L) Single optical section through the center of the proximal compartment showing the interaction of microtubules with the nucleus (N) and chloroplasts.

(M) Single optical section through the outer cortical region of the proximal compartment showing densely packed chloroplasts with a nucleus (N) among them and microtubules interweaving around these organelles.

suggesting active mitochondrial activity and cell viability (see Supplemental Figures 4B and 4E online). Similar ER patches were also observed in CD-treated onion (*Allium cepa*) epidermal cells (Knebel et al., 1990). This treatment resulted in the disruption of the actin cytoskeleton but not the tubulin cytoskeleton, as indicated by immunofluorescence results (Figures 8E and 8F). Control cells treated with 0.1% DMSO, which was used in the drug treatments, showed no significant difference in organelle arrangement from untreated cells (Figures 8A to 8C).
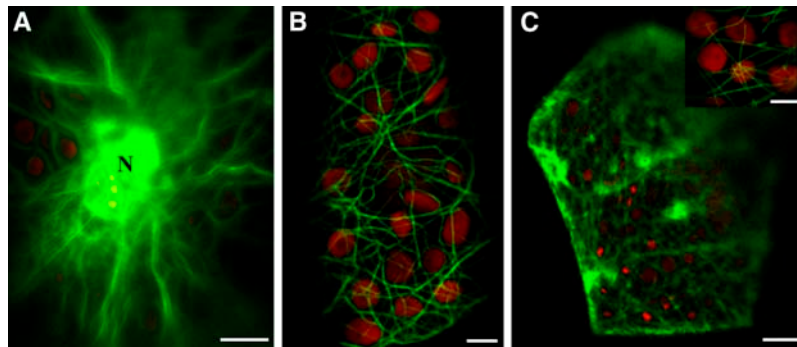
Figure 7. Live Cell Localization of GFP Fusion Proteins.

B. sinuspersici chlorenchyma cells transiently expressing GFP chimeric proteins to actin binding protein (talin) or MAP4. Bars = 10 μm in **(A)** and **(C)** and 5 μm in **(B)** and inset in **(C)**.

(A) Chlorenchyma cell transformed with GFP-talin showing thick actin filament bundles extending from the nucleus (N) and the CCC.

(B) Closeup image of a chlorenchyma cell transformed with GFP-talin showing actin filaments interacting with chloroplasts in the cortical region.

(C) Chlorenchyma cell transformed with GFP-MAP4 showing a dense network of microtubules in the cortical region. The inset shows an optical section through the cortical region of a GFP-MAP4–expressing cell showing both microtubules and chloroplasts.

The arrangement of chloroplasts in *S. aralocaspica* chlorenchyma cells was not as dramatically affected by these cytoskeleton-depolymerizing drugs. This could possibly be attributable to the inability of the drugs to penetrate the tightly packed chlorenchyma cells. Figures 9A to 9C depict cells incubated in solution containing 0.1% DMSO to show the usual cytoskeletal patterns of control *S. aralocaspica* cells. Most *S. aralocaspica* chlorenchyma cells treated with CD showed no obvious changes in organelle arrangement (Figures 9D to 9F). However, most Ory-treated *S. aralocaspica* cells showed changes in chloroplast distribution, displaying clustering of chloroplasts in the distal compartment (Figures 9G to 9I). Immunofluorescence labeling showed that these drug treatments did in fact disrupt the respective cytoskeleton elements (Figure 9I). To further determine whether there were interactions between the two cytoskeleton systems with respect to chloroplast anchoring in *S. aralocaspica*, leaf sections were exposed to a combination of actin filament– and microtubule-disrupting drugs. Treatment with both CD and Ory caused significant dispersal of chloroplasts in most cells. The chloroplasts in the distal region appeared in clusters, whereas the tightly packed proximal chloroplasts became slightly dispersed (Figures 9J to 9L).

DISCUSSION

In this study, we provide important information on both organelle distribution and possible mechanisms for the maintenance of this pattern of distribution to achieve cellular function in the two known types of terrestrial single-cell C$_4$ photosynthesis. The chlorenchyma cells of *Bienertia* and *S. aralocaspica* are remarkable in their ability to carry out C$_4$ photosynthesis without a dual cell system, as has been the paradigm for terrestrial plant C$_4$ photosynthesis (Edwards et al., 2004). The partitioning of structurally and biochemically dimorphic chloroplasts, as shown previously (Voznesenskaya et al., 2001), is important to the single-cell operation of C$_4$, but this is only one part of the cycle. These single-cell C$_4$ photosynthetic systems present some fas-

cinating problems with respect to their regulation, including the induction of the C$_4$ cycle carbon-concentrating mechanism and their effective operation in the absence of Kranz anatomy. In mature chlorenchyma cells of each genus, there is a clear compartmentalization of enzymes and organelles that are relevant to the C$_4$ cycle. Both *Bienertia* and *S. aralocaspica* are NAD-ME–type C$_4$ species, as shown here and elsewhere (Voznesenskaya et al., 2001, 2002, 2005). In species with Kranz anatomy, enzymes that function in bundle sheath cells include NAD-ME, which is localized in mitochondria, and glycolate oxidase and glycine decarboxylase of the photorespiratory pathway, which are located in peroxisomes and mitochondria, respectively (Edwards and Walker, 1983).

This study demonstrates that mitochondria are permanently partitioned to distinct subcellular regions in each of the single-cell C$_4$ species to concentrate CO$_2$ around Rubisco-containing chloroplasts. The partitioning of mitochondria permits the efficient mobilization of other mitochondrial functions in these regions of high energy demand required for CO$_2$ assimilation. In both genera, the peroxisomes are also partitioned preferentially to the compartments with mitochondria and Rubisco-containing chloroplasts. However, the results for peroxisome dynamics in *Bienertia* suggest the existence of two types of peroxisomes. The static peroxisomes in the central and proximal compartments of *Bienertia* and *S. aralocaspica*, respectively, are most likely involved in the glycolate pathway along with mitochondria to trap any residual CO$_2$ generated from photorespiration that may occur in these single-cell systems. By contrast, the mobile peroxisomes may be involved in other metabolic processes that are essential for developmental and differentiation programs. This cellular organization confines the generation of CO$_2$ to the C$_4$ pathway and from any photorespiration that occurs to the bundle sheath cells, which is critical to the function of C$_4$ photosynthesis.

The mechanisms responsible for stabilizing and maintaining this polarized distribution of organelles are also critical to these unique photosynthetic systems. The cytoskeleton is involved in
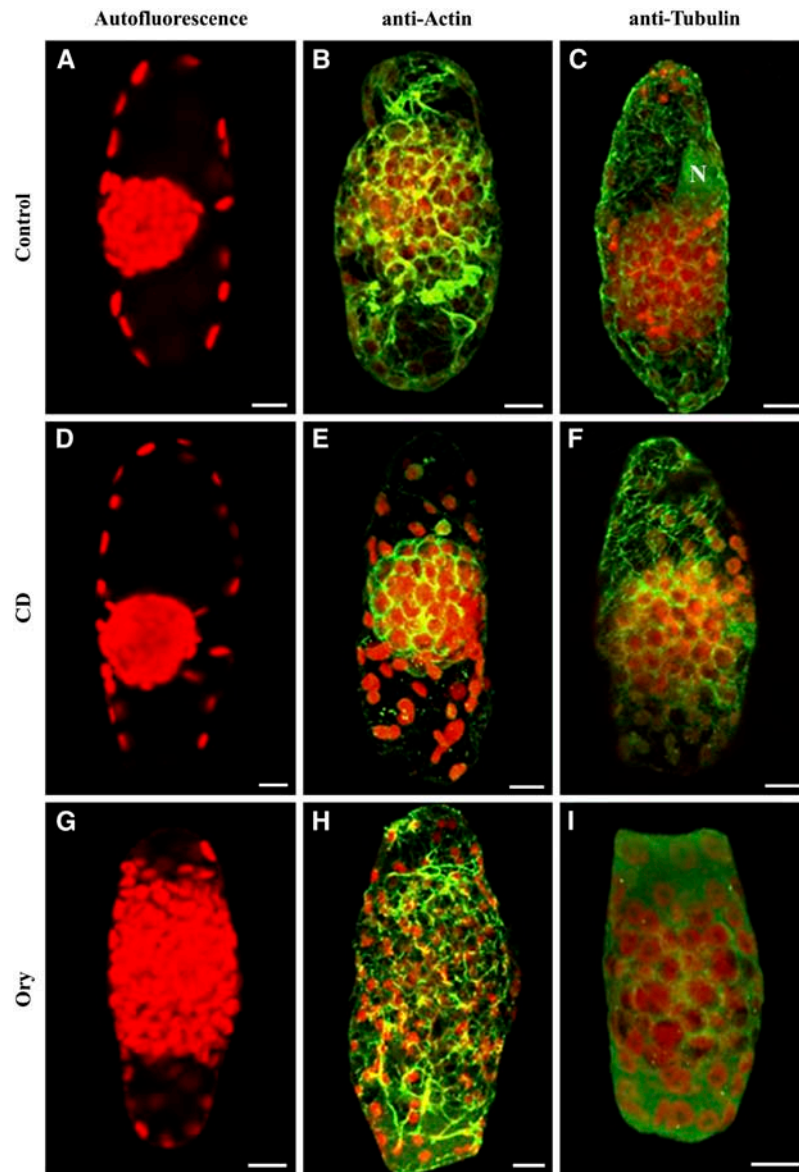
Figure 8. Effects of CD and Ory on the Organization of the Central Cytoplasmic Compartment in *B. sinuspersici* Chlorenchyma Cells.

(A), **(D)**, and **(G)** Autofluorescence of chloroplasts of chlorenchyma cells incubated over a 2-h period in stabilizing buffer **(A)** and in the same buffer containing 100 μM CD **(D)** or 30 μM Ory **(G)**.
(B) and **(C)** Control chlorenchyma cells were fixed and probed with anti-actin **(B)** or anti-tubulin **(C)** antiserum to test the effects of the drugs on the two cytoskeletal elements.
(E) and **(F)** CD-treated cells probed with actin and tubulin antibodies showing complete disruption of actin filaments **(E)** with intact microtubules **(F)**.
(H) and **(I)** Ory-treated chlorenchyma cells with dispersed CCC. The actin filaments remain intact **(H)**, whereas microtubules are completely disrupted **(I)**. These are representative results from at least three separate experiments. Bars = 10 μm.

various cellular processes, including the generation and maintenance of cell shape, organelle movement, and the anchoring and general transport of organelles and macromolecules throughout the cell (Wasteneys and Galway, 2003). The maintenance of organelle compartmentalization in the single-cell C_4 systems suggests the involvement of the cytoskeleton, as shown here by the demonstration of the close interaction between chloroplasts and actin filaments and microtubules and by the results of pharmacological studies. In mature chlorenchyma cells of *Bienertia* and *S. aralocaspica*, the cytoskeleton network is quite extensive. Chloroplasts either align directly along thick actin cables or are attached to the thin actin filaments connected to the cables. In addition, the chloroplasts are partly or completely surrounded by rings or baskets of both actin filaments and microtubules. These observations suggest a role for direct interactions between the organelle and the cytoskeleton or
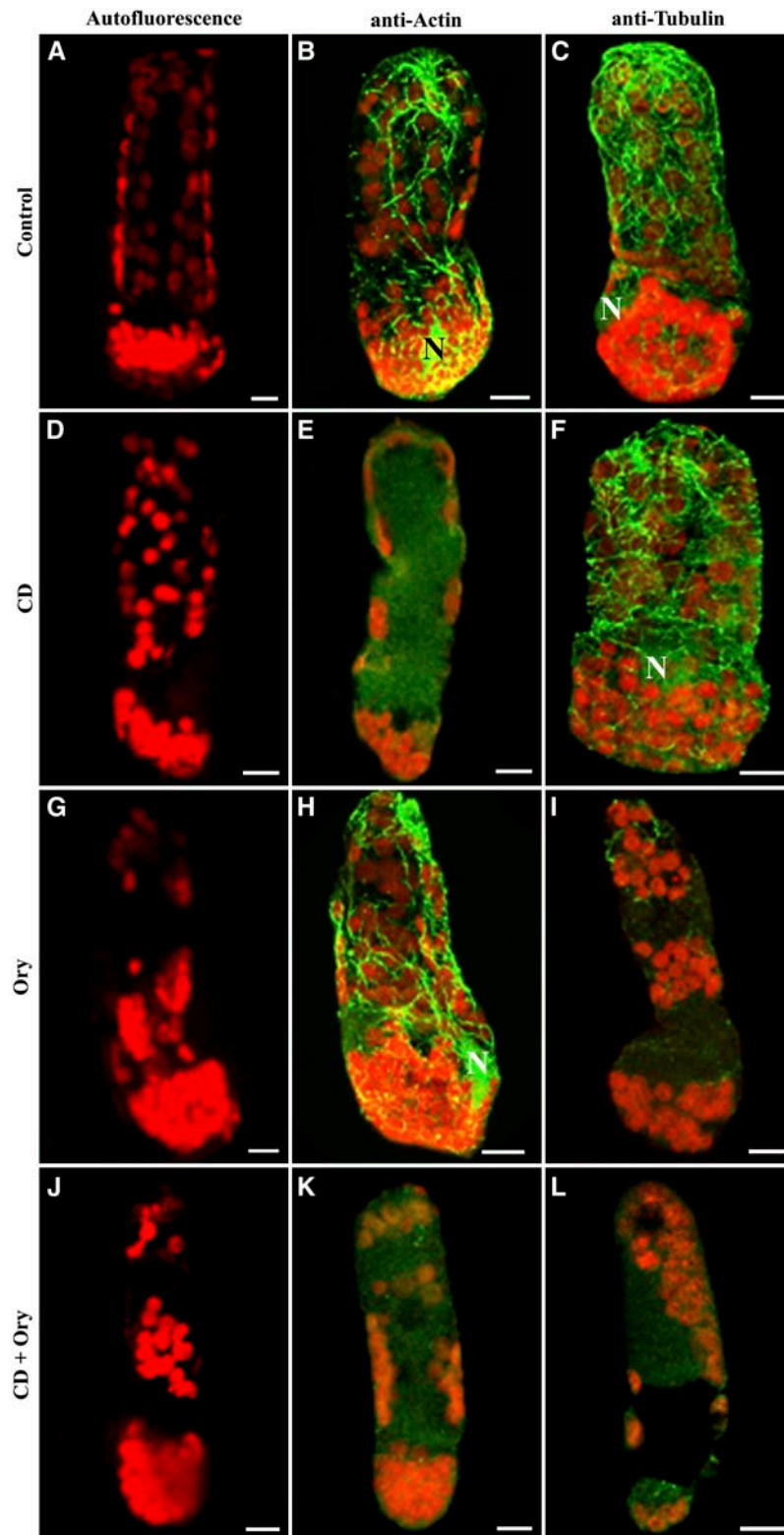
Figure 9. Effects of CD and Ory on the Distribution of Chloroplasts in the Two Cellular Compartments of *S. aralocaspica* Chlorenchyma Cells.

(A), **(D)**, **(G)**, and **(J)** Autofluorescence images of chlorenchyma cells incubated over a 2-h period in stabilizing buffer **(A)** and in the same buffer containing 100 μM CD **(D)**, 30 μM Ory **(G)**, or a combination of both drugs **(J)**.

indirectly via cytoskeleton-associated proteins. However, our observations do not rule out artifacts in the arrangement of the cytoskeleton induced by chemical fixation. Although this is a possibility, the cytoskeletal patterns appear authentic, as studies using transient expression of a GFP–cytoskeletal protein chimera in living *Bienertia* cells further reveal similar extensive cytoskeletal arrangements.

Relevant to our study, a role of actin filaments in chloroplast positioning or movement has been demonstrated in plants (Kandasamy and Meagher, 1999; Oikawa et al., 2003). For example, in *Arabidopsis*, baskets of actin filaments have been observed surrounding the chloroplasts, and disruption of these filaments by latrunculin B resulted in a disorganization of the intracellular arrangement of chloroplasts (Kandasamy and Meagher, 1999). Similarly, the intracellular movement of chloroplasts in many cells, including algae, mosses, ferns, and angiosperms, has been shown to be inhibited by antiactin drugs (Witztum and Parthasarathy, 1985; Menzel and Schliwa, 1986; Kadota and Wada, 1992; Nagai, 1993; Dong et al., 1996; Sato et al., 2001). These studies suggest that actin filaments play a major role in the positioning and movement of chloroplasts. Although most studies of higher plants have demonstrated that actin filaments are the predominant structure controlling chloroplast movement and positioning, other studies have demonstrated that microtubules have a role in organelle movement (Wada et al., 2003; Wada and Suetsugu, 2004). Studies of this type on plants and macroalgae have dealt specifically with changes in chloroplast position in response to light intensity. The single-cell C_4 systems appear unique in that, early in leaf development, chloroplasts become separated into two cytoplasmic compartments and thereafter remain anchored (Voznesenskaya et al., 2003, 2005). This partitioning of chloroplasts in mature chlorenchyma cells does not change during the night or under different light conditions (E. Voznesenskaya, N. Koteyeva, S.D.X. Chuong, V.R. Franceschi, and G.E. Edwards, unpublished data). Thus, it appears that the signaling pathways that operate during organelle compartmentalization in these single-cell systems may involve different mechanisms than those observed for the photoreceptor-induced chloroplast movement seen in *Arabidopsis thaliana*.

Although it is premature to describe the functions of the cytoskeleton, it is possible to speculate some general roles from our observations. The interactions of chloroplasts with these cellular arrays suggest a role for actin filaments and microtubules in the cellular movement of chloroplasts in response to developmental or environmental stimuli, whereas the presence of baskets of actin filaments and microtubules around the chloroplasts

implies a role for these cytoskeletal structures in anchoring them to their respective compartments or in controlling organelle morphology. However, the molecular mechanisms involved in this interaction remain to be determined. Similar observations have been documented in etiolated tobacco (*Nicotiana tabacum*) hypocotyls, suggesting that nongreen plastid morphology and dynamics are dependent on both actin filaments and microtubules (Kwok and Hanson, 2003). Because plastids serve as sites of many important biochemical reactions, the cytoskeletal networks may also serve as tracks to facilitate the exchange of metabolites between plastids and the cytosol or other organelles, a critical factor in the efficiency of cellular metabolism.

To determine the role of actin filaments and microtubules in stabilizing the organelle polarization required for single-cell C_4 photosynthesis to operate, we examined the effects of two cytoskeleton-disrupting drugs, CD and Ory, specific inhibitors of actin and tubulin polymerization, respectively, on the maintenance of chloroplasts in distinct cellular compartments. Treatment of *Bienertia* cells with the microtubule-depolymerizing drug Ory resulted in a dispersion of the chloroplasts in the CCC, whereas the actin-disrupting drug CD did not, suggesting that the integrity of this compartment is dependent on microtubules. This dispersion of chloroplasts results from the absence of intact microtubules, because labeling of the Ory-treated cells with tubulin or actin antibody revealed that the tubulin network is disrupted, whereas the actin filaments were unaffected. This also suggests that the stabilization of the large spherical CCC, which is essentially positioned in the vacuole, requires a more robust and rigid structure possibly associated with a microtubular cage. Therefore, the maintenance of organelle compartmentalization in *Bienertia* appears to be a predominantly microtubule-dependent process. Similarly, a recent study demonstrates that the movement of nongreen plastids involves actin filaments, whereas microtubules serve to restrain their movement (Kwok and Hanson, 2003). This observation is consistent with our results, which show that although CD disrupts actin filaments, the cellular distribution of chloroplasts is not affected. Moreover, in tobacco cells, mitochondrial movement is dependent on an intact F-actin–myosin system, whereas their positioning in the cortical cytoplasm involves both cytoskeletal networks (Van Gestel et al., 2002; Logan et al., 2003). Altogether, these studies provide additional support implicating a role for microtubules in the positioning of organelles in plant cells.

In *S. aralocaspica*, treatment of cells with Ory resulted in a moderate aggregation of chloroplasts in the distal compartment. However, treatment involving a combination of both actin-disrupting and microtubule-depolymerizing drugs induced

---

Figure 9. (continued).

(B) and **(C)** Control chlorenchyma cells were fixed and probed with anti-actin **(B)** or anti-tubulin **(C)** antiserum to demonstrate the effectiveness of the drugs on the two cytoskeletal elements.
(E) and **(F)** CD-treated cells showing the complete disruption of actin filaments **(E)**, but the transverse orientation of microtubules is not affected **(F)**.
(H) and **(I)** Ory-treated chlorenchyma cells showing intact actin filaments **(H)** and complete disruption of microtubules **(I)**.
(K) and **(L)** CD- and Ory-treated chlorenchyma cells showing complete disruption of both cytoskeleton systems and the aggregation of chloroplasts in the distal compartment.
These are representative results from at least three independent experiments. Bars = 10 μm.

further clustering of chloroplasts. These studies further suggest a role for microtubules in the partitioning of chloroplasts to distinct cellular compartments within the chlorenchyma cell. Actin filaments may have an additional role in maintaining organelle position in *S. aralocaspica*. This species has chloroplasts and other organelles packed between the cell wall and the vacuole, so that at least one surface is relatively permanent and of greater mechanical capacity. Therefore, it has less need for an extensive microtubular cage like that found in the central cytoplasmic compartment in *Bienertia*, which has only the tonoplast and pressure from the vacuole to stabilize it. Interactions between actin filaments and microtubules in plant cells are well documented (Gavin, 1997; Blancaflor, 2000; Collings and Allen, 2000; Samaj et al., 2000). For example, immunofluorescence and immunoelectron analyses showed that microtubules and actin filaments often colocalize in plant cells, suggesting that these structural components interact with each other (Lancelle and Hepler, 1989). Moreover, microtubules and actin filaments are integrated structures that make up the preprophase band, mitotic spindle, and phragmoplast in plant cells. In maize (*Zea mays*) root cells, an interaction between actin filaments and microtubules was also demonstrated (Blancaflor, 2000).

The close interrelationship of the actin and microtubule cytoskeletal systems with organelles such as chloroplasts raises the possibility that a given organelle could depend on both types of filament for positioning or movement. Although our data do not reveal which cytoskeletal element, actin filaments or microtubules, interacts first with the organelles at the onset of cellular organization, our observations do indicate that the spatial distribution of actin filaments and microtubules is coordinately regulated during organelle partitioning. The complex patterns we see associating with chloroplasts and other organelles further indicate that the two cytoskeletal systems are physically linked to each other and that these dense cytoskeletal networks could inhibit the movement of organelles by physically restricting their movement. Therefore, we hypothesize that the actin-based system provides the mechanism of moving organelles during the early stage of organelle partitioning and fine-tunes their positioning in mature cells, whereas the microtubule-based system maintains the proper spatial relationships of organelles at a given subcellular location. These data also suggest that organelles could possess multiple types of motor proteins or cytoskeleton-associated proteins allowing them to be associated directly or indirectly with both actin filaments and microtubules. The former association would be used for mobility, whereas the latter would result in organelle immobilization. However, the molecular factors of these interactions remain to be identified. Besides controlling the partitioning of organelles, the cytoskeleton may also be involved in directing the movement or localization of nonorganelle cellular components.

In summary, this study demonstrates that the organelle polarization in the two different single-cell C$_4$ systems extends beyond the chloroplasts, as shown previously, to include mitochondria, nuclei, and peroxisomes. Given the enzymes present in these organelles, this intracellular compartmentalization appears to be essential for the efficient operation of the system. The data from this study, showing the close interaction between cytoskeletal components and organelles, support other recent studies suggesting that these cellular arrays are essential structures for numerous plant intracellular transport activities, such as macromolecule trafficking, metabolic channeling, and signaling (Kost et al., 2002; Chuong et al., 2004; Wasteneys and Yang, 2004). The evidence presented here indicates that the cytoskeleton, especially microtubules, is required for the structural integrity of the unique compartmentalization required for the single-cell C$_4$ systems and also is likely involved in establishing the biochemical polarity, through trafficking of molecular species to the appropriate compartment. Future work will focus on this latter potential process as well as the mechanisms by which the organelles are moved to their respective positions during the development of the cells. Although the answer is not known, a potential player in these processes is the cytoskeleton.

METHODS

Plant Material and Growth Conditions

Seeds of *Bienertia sinuspersici* (Akhani et al., 2005) and *Suaeda aralocaspica* (formerly *Borszczowia aralocaspica*) (Schütze et al., 2003; Voznesenskaya et al., 2003) were germinated on moist filter paper at room temperature. Seedlings were then transferred to 4-inch pots containing a soil mixture of 2 parts commercial potting soil, 1 part clay soil, 1 part sand, 0.5 parts Perlite, and 0.5 parts dolomite powder and were watered three times per week and once every week with Miracle-Grow Excel 21-5-20 fertilizer and a salt solution (0.150 M NaCl). Plants were grown in controlled-environment chambers (model GC-16; Enconair Ecological Chambers) with day/night temperatures of 25/15°C and a 14-/10-h photoperiod, with a stepwise increase and decrease in light intensity during the day to a maximum photosynthetic photon flux density of 1100 μmol$\cdot$m$^{-2}\cdot$s^{-1}. Mature leaves from 4- to 6-month-old plants were used for analyses.

Light Microscopy

Samples for anatomical studies were fixed for 10 to 11 h at 4°C in 2% (v/v) paraformaldehyde and 2% (v/v) glutaraldehyde in 0.1 M phosphate buffer, pH 7.2, postfixed in 4% (w/v) OsO$_4$, and then after a standard acetone dehydration procedure, embedded in Spurr's epoxy resin. Cross sections were made on a Reichert Ultracut R ultramicrotome (Reichert-Jung). For light microscopy, semithin sections were stained with 1% (w/v) toluidine blue O in 1% (w/v) Na$_2$B$_4$O$_7$.

In Situ Immunolocalization

Leaf samples were fixed at 4°C in 2% (v/v) paraformaldehyde and 1.25% (v/v) glutaraldehyde in 0.05 M PIPES buffer, pH 7.2. The samples were dehydrated with a graded ethanol series and embedded in London Resin White (Electron Microscopy Sciences) acrylic resin. Antibodies used (all raised in rabbit) were anti–*Spinacea oleracea* Rubisco large subunit (courtesy of B. McFadden), anti–*Zea mays* PPDK (courtesy of T. Sugiyama), and anti–*Sorghum vulgare* NADP-MDH (courtesy of M. Miginiac-Maslow). As a negative control, sections were treated as described below except that the primary antibodies were omitted.

Cross sections (0.8 to 1 μm thick) were dried in a drop of water on gelatin-coated slides and blocked for 1 h with TBST + BSA (10 mM Tris-HCl, 0.15 M NaCl, 0.1% [v/v] Tween 20, and 1% [w/v] BSA, pH 7.2). They were then incubated for 3 h with anti-Rubisco (1:500 dilution), anti-PPDK (1:200), or anti-NADP-MDH (1:100) antibody diluted in TBST + BSA. The slides were washed with TBST + BSA and then treated for 1 h with protein A–gold (10-nm particles diluted 1:100 with TBST + BSA). After washing,

the sections were exposed to a silver-enhancement reagent for 20 min according to the manufacturer's directions (Amersham), stained with 0.5% (w/v) Safranin O, and imaged in reflected/transmitted mode using a Bio-Rad 1024 confocal system with a Nikon Eclipse TE 300 inverted microscope and Lasergraph imaging program 3.10 (Bio-Rad). The experiments were repeated at least three times each with triplicate samples.

Organelle Labeling

Live cells were used for visualization of the ER, mitochondria, nuclei, and vacuole. Vibratome leaf sections (100 μm thick) of *S. aralocaspica* were made with a series 1000 vibratome (Technical Products International). For the preparation of isolated *Bienertia* chlorenchyma cells, the epidermis was removed with a fine-tip forceps and chlorenchyma cells were released and collected in PME buffer (0.05 M PIPES, 5 mM $MgSO_4$, and 5 mM EGTA) supplemented with 0.5 M mannitol and 0.15 M NaCl. The ER and vacuole were stained for 15 min with 5 μM $DiOC_6(3)$ (Sigma-Aldrich) and carboxy-DCFCA (Molecular Probes), respectively. Mitochondria and nuclei were stained for 30 min with 10 μg/mL rhodamine 123 and acridine orange (Sigma-Aldrich), respectively. Isolated cells and leaf sections were stained in PME buffer containing the appropriate concentrations of fluorescent dyes followed by two 10-min rinses in PME buffer before confocal microscope imaging. Results presented were repeated at least three times independently with similar results.

Protein Extraction and Protein Gel Blot Analysis

Total proteins were extracted from mature leaves by homogenizing 0.5 g of tissue in 1 mL of extraction buffer (0.1 M Tris-HCl, pH 7.5, 5 mM $MgSO_4$, 10 mM DTT, 5 mM EDTA, 0.5% [w/v] SDS, 2% [v/v] β-mercaptoethanol, 10% [v/v] glycerol, 1 mM phenylmethylsulfonyl fluoride, and 2.5 μg/mL each of aprotinin, leupeptin, and pepstatin). After centrifugation at 14,000 rpm for 3 min in a microcentrifuge, the supernatant was collected and protein concentration was determined with the Bradford protein assay (Bio-Rad) using BSA as a standard. Protein samples (10 μg) were separated by 12% (v/v) SDS-PAGE, transferred to nitrocellulose, blocked in TBST containing 1% (w/v) BSA, and probed with antisera raised against *Amaranthus hydrochondriacus* mitochondrial NAD-ME (courtesy of J. Berry; 1:5000), *Z. mays* PEPC IgG (Chemicon; 1:60,000), *Z. mays* PPDK (1:10,000), *S. oleracea* Rubisco (1:40,000), chicken gizzard skeletal actin (clone C4; ICN Biomedicals; 1:3000), and bovine β-tubulin (T4026; Sigma-Aldrich; 1:3000) overnight at 4°C. Goat anti-rabbit IgG alkaline phosphatase–conjugated secondary antibody (Bio-Rad) at a dilution of 1:30,000 was used for the detection of the enzymes. Blots were developed with 350 μg/mL nitroblue tetrazolium and 175 μg/mL 5-bromo-4-chloro-3-indolyl phosphate in detection buffer (100 mM Tris-HCl, pH 9.5, 100 mM NaCl, and 5 mM $MgCl_2$).

Immunofluorescence Microscopy

Isolated *Bienertia* chlorenchyma cells and *S. aralocaspica* leaf sections were fixed in 4% (v/v) paraformaldehyde and 0.05% (v/v) glutaraldehyde solution in PME buffer for 30 min followed by washing three times in PME. The cells were then incubated for 30 min at room temperature in cell wall digestion solution preheated at 37°C (1% [w/v] cellulase [Worthington], 0.1% [w/v] pectolyase [Sigma-Aldrich], 0.3 M mannitol, 0.5% [v/v] Triton X-100, 1 mM phenylmethylsulfonyl fluoride, and 20 μg/mL each of aprotinin, leupeptin, and pepstatin) in PME, followed by two washes in PME. Cells were subsequently immersed in cold methanol for 5 min to stop the enzyme reaction. After three washes in PBS, cells were blocked with PBS buffer containing 1% (w/v) BSA for 1 h followed by an overnight incubation at 4°C with the appropriate primary antibodies in PBS containing 1% (w/v) BSA. The β-tubulin and anti-actin monoclonal antibodies were used at dilutions of 1:300 to label microtubules and

actin filaments, respectively. A monoclonal anti-catalase antibody (courtesy of R. Mullen; 1:500) was used to label peroxisomes. After primary antibody treatment, cells were washed three times in PBS containing 0.05% (v/v) Tween 20 (PBST) and then incubated for 2 h with Oregon green–conjugated anti-mouse secondary antibody (Molecular Probes; 1:400) in PBS containing 1% (w/v) BSA followed by three washes with PBST. Cells were mounted on a glass slide in 50% (v/v) glycerol in Tris, pH 9.5, containing an antifade reagent (Bio-Rad). Experiments were repeated at least five times. In most experiments, ~50% of the cells showed generally good cytoskeleton preservation, although some cells did not display uniform cytoskeletal labeling, most likely as a result of antibody penetration.

Drug Treatments

Preliminary experiments were conducted to determine the most effective and reproducible concentrations of cytoskeleton-disrupting drugs. Stock concentrations of 10 mM CD (Sigma-Aldrich) and 50 mM Ory (Cresent Chemical) were made in DMSO. Final drug concentrations used were 100 μM CD and 30 μM Ory. Appropriate amounts of stock solutions were diluted to experimental concentrations in PME buffer containing 0.5 M mannitol with DMSO added to give a final concentration of 0.1% (v/v) DMSO. All negative control experiments were conducted with a 0.1% (v/v) DMSO solution. *Bienertia* chlorenchyma cells were treated with drugs for 2 h, whereas *S. aralocaspica* leaf sections required a 4-h incubation period before experimental observations were made. The samples were immediately fixed and processed as described above for immunofluorescence experiments. Recovery observations were made with isolated *Bienertia* chlorenchyma cells. Drugs were removed with several rinses in PME buffer containing 0.5 M mannitol, and cell viability was monitored for up to 24 h after rinsing by observing the uptake of $DiOC_6(3)$ and rhodamine 123.

Scanning Electron Microscopy

Mature leaves were cut directly into fixative composed of 2% (v/v) paraformaldehyde and 1.25% (v/v) glutaraldehyde in PME buffer. After 1 h of fixation, samples were frozen in liquid nitrogen, cryofractured, and permeabilized for 1 h with 1% (v/v) Triton X-100 in PME buffer. After two washes in PBS, the samples were postfixed in 0.5% (w/v) osmium tetroxide at room temperature for 2 h, washed in PME, and dehydrated in a standard ethanol series to 100%. The samples were then critical-point-dried, mounted onto scanning electron microscope stubs, sputter-coated with gold, and observed with a Hitachi S570 scanning electron microscope (Hitachi Scientific Instruments).

Biolistic Transformation of *Bienertia* Chlorenchyma Cells

Biolistic transformation of chlorenchyma cells in intact *Bienertia* leaves was done with tungsten particles coated with plasmids containing the actin binding protein talin-GFP (Kost et al., 1998), MAP4-GFP gene fusion (Marc et al., 1998), or MFP-GFP gene fusion (Chuong et al., 2005). Briefly, 5 μg of plasmid was purified using the Qiagen plasmid DNA purification kit and mixed in a suspension of 1 mg of tungsten (1 μm; Bio-Rad), 0.1 M $CaCl_2$, and 16 mM spermidine. The mixture was vortexed continuously for 2 min, and the DNA-coated tungsten particles were collected by brief centrifugation, washed in 70 and 100% ethanol, resuspended in 100% ethanol, and loaded onto the plastic macrocarrier discs (Bio-Rad). The DNA-coated tungsten particles were bombarded into *Bienertia* leaves from a distance of 10 cm using a Biolistic PDS-1000/He particle-delivery system (Bio-Rad) at a helium pressure of 1350 p.s.i. The bombarded leaves were placed in Petri dishes on moist filter paper and stored at room temperature under ambient light for 16 h before microscopic observation.

Confocal Microscopy

Confocal microscopy was performed on a Bio-Rad MRC 1024 laser scanning confocal microscope with a Nikon Eclipse TE 300 inverted microscope (Bio-Rad). Images were acquired through a 40× Zeiss Plan-Apochromat oil-immersion objective at a maximum digital resolution of 512 × 512. The fluorescence of Oregon green–conjugated secondary antibody, GFP, DiOC$_6$(3), carboxy-DCFDA, rhodamine 123, and acridine orange was excited at 488 nm, and emission was detected between 500 and 550 nm. Chlorophyll fluorescence was excited at 594 nm, and emission was detected between 600 and 700 nm. Serial optical sections were obtained at 0.8-μm intervals in the z axis using the Lasergraph 3.10 imaging software (Bio-Rad). Image processing was performed using Adobe Photoshop. Images of at least 10 cells were obtained from each individual experiment.

Supplemental Data

The following materials are available in the online version of this article.

Supplemental Figure 1. Detergent-Resistant Components in *B. sinuspersici* and *S. aralocaspica* Chlorenchyma Cells.

Supplemental Figure 2. Specificity of the Anti-Actin and Anti-Tubulin Antibodies.

Supplemental Figure 3. The Actin and Microtubule Cytoskeleton in Chlorenchyma Cells of *S. heterophylla* (C$_3$) and *S. eltonica* (C$_4$ Kranz).

Supplemental Figure 4. Effects of CD and Ory on *Bienertia* Chlorenchyma Cell Viability.

REFERENCES

Akhani, H., Barroca, J., Koteeva, N.K., Voznesenskaya, E., Franceschi, V., Edwards, G., Ghaffari, S., and Ziegler, H. (2005). *Bienertia sinuspersici* (Chenopodiaceae): A new species from Southwest Asia and discovery of a third terrestrial C$_4$ plant without Kranz anatomy. Syst. Bot. **30,** 290–301.

Blancaflor, E.B. (2000). Cortical actin filaments potentially interact with cortical microtubules in regulating polarity of cell expansion in primary roots of maize (*Zea mays* L.). J. Plant Growth Regul. **19,** 406–414.

Boevink, P., Oparka, K., Cruz, S.S., Martin, B., Betteridge, A., and Hawes, C. (1998). Stacks on tracks: The plant Golgi apparatus traffics on an actin/ER network. Plant J. **3,** 441–447.

Chuong, S.D., Good, A.G., Taylor, G.J., Freeman, M.C., Moorhead, G.B., and Muench, D.G. (2004). Large-scale identification of tubulin-binding proteins provides insight on subcellular trafficking, metabolic channeling, and signaling in plant cells. Mol. Cell. Proteomics **3,** 970–983.

Chuong, S.D.X., Park, N.I., Freeman, M.C., Mullen, R.T., and Muench, D.G. (2005). The peroxisomal multifunctional protein interacts with cortical microtubules in plant cells. BMC Cell Biol. **6,** 40.

Chytilova, E., Macas, J., Sliwinska, E., Rafelski, S.M., Lambert, G.M., and Galbraith, D.W. (2000). Nuclear dynamics in *Arabidopsis thaliana.* Mol. Biol. Cell **11,** 2733–2742.

Collings, D., Harper, J., Marc, J., Overall, R., Mullen, R., Jedd, G., and Chua, N.-H. (2002). Life in the fast lane: Actin-based motility of plant peroxisomes. Plant Cell Physiol. **43,** 430–441.

Collings, D.A., and Allen, N.S. (2000). Cortical actin interacts with the plasma membrane and microtubules. Dev. Plant Soil Sci. **89,** 145–164.

Dong, X.-J., Ryu, J.-H., Takagi, S., and Nagai, R. (1996). Dynamic changes in the organization of microfilaments associated with the photocontrolled motility of chloroplasts in epidermal cells of *Vallisneria.* Protoplasma **195,** 18–24.

Edwards, G.E., Franceschi, V.R., Ku, M.S.B., Voznesenskaya, E.V., Pyankov, V.I., and Andreo, C.S. (2001a). Compartmentation of photosynthesis in cells and tissues of C$_4$ plants. J. Exp. Bot. **52,** 577–590.

Edwards, G.E., Franceschi, V.R., and Voznesenskaya, E.V. (2004). Single cell C$_4$ photosynthesis versus the dual-cell (Kranz) paradigm. Annu. Rev. Plant Physiol. Plant Mol. Biol. **55,** 173–196.

Edwards, G.E., Furbank, R.T., Hatch, M.D., and Osmond, C.B. (2001b). What does it take to be C$_4$? Lessons from the evolution of C$_4$ photosynthesis. Plant Physiol. **125,** 46–49.

Edwards, G.E., and Huber, S.C. (1981). The C$_4$ pathway. In The Biochemistry of Plants: A Comprehensive Treatise. Vol. 8. Photosynthesis, M.D. Hatch and N.K. Boardman, eds (New York: Academic Press), pp. 237–281.

Edwards, G.E., and Walker, D.A. (1983). C$_3$, C$_4$: Mechanisms, and Cellular and Environmental Regulation, of Photosynthesis. (Oxford, UK: Blackwell Scientific Publications).

Freitag, H., and Stichler, W. (2000). A remarkable new leaf type with unusual photosynthetic tissue in a Central Asiatic genus of Chenopodiaceae. Plant Biol. **2,** 154–160.

Freitag, H., and Stichler, W. (2002). *Bienertia cycloptera* Bunge ex Boiss., Chenopodiaceae, another C$_4$ plant without Kranz tissues. Plant Biol. **4,** 121–132.

Gavin, R.H. (1997). Microtubule-microfilament synergy in the cytoskeleton. Int. Rev. Cytol. **173,** 207–242.

Hatch, M.D. (1971). Mechanism and function of C$_4$ photosynthesis. In Photosynthesis and Photorespiration, M.D. Hatch, C.B. Osmond, and R.O. Slatyer, eds (New York: Wiley-Interscience), pp. 139–152.

Hatch, M.D., Osmond, C.B., and Slatyer, R.O., eds (1971). Photosynthesis and Photorespiration. (New York: Wiley Interscience).

Hatch, M.D., and Slack, C.R. (1970). Photosynthetic CO$_2$-fixation pathways. Annu. Rev. Plant Physiol. **21,** 141–163.

Jedd, G., and Chua, N.H. (2002). Visualization of peroxisomes in living plant cells reveals acto-myosin-dependent cytoplasmic streaming and peroxisome budding. Plant Cell Physiol. **4,** 384–392.

Kadota, A., and Wada, M. (1992). Photoinduction of formation of circular structures by microfilaments on chloroplasts during intracellular orientation in protonemal cells of the fern *Adiantum capillus-veneris.* Protoplasma **167,** 97–107.

Kandasamy, M.K., and Meagher, R.B. (1999). Actin-organelle interaction:

Association with chloroplast in *Arabidopsis* leaf mesophyll cells. Cell Motil. Cytoskeleton **44,** 110–118.

Kapralov, M.V., Akhani, H., Voznesenskaya, E.V., Edwards, G.E., Franceschi, V.R., and Roalson, E.H. (2006). Phylogenetic relationships in the Salicornioideae/Suaedoideae/Salsoloideae s.l. (Chenopodiaceae) clade and a clarification of the phylogenetic position of *Bienertia* and *Alexandra* using multiple DNA sequence datasets. Syst. Bot. **31,** 571–585.

Knebel, W., Quader, H., and Schnepf, E. (1990). Mobile and immobile endoplasmic reticulum in onion bulb epidermis cells: Short- and long-term observations with a confocal laser scanning microscope. Eur. J. Cell Biol. **52,** 328–340.

Kost, B., Bao, Y.-Q., and Chua, N.-H. (2002). Cytoskeleton and plant organogenesis. Philos. Trans. R. Soc. Lond. B Biol. Sci. **357,** 777–789.

Kost, B., Spielhofer, P., and Chua, N.-H. (1998). A GFP-mouse talin fusion protein labels plant actin filaments in vivo and visualizes the actin cytoskeleton in growing pollen tubes. Plant J. **3,** 393–401.

Ku, M.S.B., Agarie, S., Nomura, M., Fukayama, H., Tsuchida, H., Ono, K., Hirose, S., Toki, S., Miyao, M., and Matsuoka, M. (1999). High-level expression of maize phosphoenolpyruvate carboxylase in transgenic rice plants. Nat. Biotechnol. **17,** 76–80.

Kuznetsov, S.A., Langford, G.M., and Weiss, D.G. (1992). Actin-dependent organelle movement in squid axoplasm. Nature **356,** 722–724.

Kwok, E.Y., and Hanson, M.R. (2003). Microfilaments and microtubules control the morphology and movement of non-green plastids and stromules in *Nicotiana tabacum.* Plant J. **35,** 16–26.

Lancelle, S.A., and Hepler, P.K. (1989). Immunogold labeling of actin on sections of freeze-substituted plant cells. Protoplasma **150,** 72–74.

Leegood, R.C. (2002). C_4 photosynthesis: Principles of CO_2 concentration and prospects for its introduction into C_3 plants. J. Exp. Bot. **53,** 581–590.

Logan, D.C., Scott, I., and Tobin, A.K. (2003). The genetic control of plant mitochondrial morphology and dynamics. Plant J. **36,** 500–509.

Mano, S., Nakamori, C., Hayashi, M., Kato, A., Kondo, M., and Nishimura, M. (2002). Distribution and characterization of peroxisomes in Arabidopsis by visualization with GFP: Dynamic morphology and actin-dependent movement. Plant Cell Physiol. **43,** 331–341.

Marc, J., Granger, C.L., Brincat, J., Fisher, D.D., Kao, T.-h., McCubbin, A.G., and Cyr, R.J. (1998). A GFP-MAP4 reporter gene for visualizing cortical microtubule rearrangements in living epidermal cells. Plant Cell **10,** 1927–1940.

Mathur, J., Mathur, N., and Hulskamp, M. (2002). Simultaneous visualization of peroxisomes and cytoskeletal elements reveals actin and not microtubule-based peroxisome motility in plants. Plant Physiol. **128,** 1031–1045.

Matsuoka, M., Furbank, R.T., Fukayama, H., and Miyao, M. (2001). Molecular engineering of C_4 photosynthesis. Annu. Rev. Plant Physiol. Plant Mol. Biol. **52,** 297–314.

Menzel, D., and Schliwa, M. (1986). Motility in the siphonous green alga *Bryopsis.* II. Chloroplast movement requires organized arrays of both microtubules and actin filaments. Eur. J. Cell Biol. **40,** 286–295.

Nagai, R. (1993). Regulation of intracellular movements in plant cells by environmental stimuli. Int. Rev. Cytol. **145,** 251–310.

Nebenfuhr, A., Gallagher, L.A., Dunahay, T.G., Frohlick, J.A., Mazurkiewicz, A.M., Meehl, J.B., and Staehelin, L.A. (1999).

Stop-and-go movements of plant Golgi stacks are mediated by the acto-myosin system. Plant Physiol. **121,** 1127–1142.

Oikawa, K., Kasahara, M., Kiyosue, T., Kagawa, T., Suetsugu, N., Takahashi, F., Kanegae, T., Niwa, Y., Kadota, A., and Wada, M. (2003). CHLOROPLAST UNUSUAL POSITIONING1 is essential for proper chloroplast positioning. Plant Cell **15,** 2805–2815.

Rogers, S.L., and Gelfand, V.I. (1998). Myosin cooperates with microtubule motors during organelle transport in melanophores. Curr. Biol. **8,** 161–164.

Rogers, S.L., and Gelfand, V.I. (2000). Cytoskeleton-membrane trafficking, organelle transport, and the cytoskeleton. Curr. Opin. Cell Biol. **12,** 57–62.

Sage, R.F. (1999). Why C4 photosynthesis? In C4 Plant Biology. Physiological Ecology Series, R.F. Sage and R.K. Monson, eds (San Diego, CA: Academic Press), pp. 3–16.

Sage, R.F. (2005). Atmospheric CO_2, environmental stress and the evolution of C_4 photosynthesis. In A History of Atmospheric CO_2 and Its Effects on Plants, Animals and Ecosystems, J.R. Ehleringer, T.E. Cerling, and D. Dearing, eds (Berlin: Springer-Verlag), pp. 185–213.

Samaj, J., Peters, M., Volkmann, D., and Baluska, F. (2000). Effects of myosin ATPase inhibitor 2,3-butanedione 2-monoxime on distributions of myosins, F-actin, microtubules and cortical endoplasmic reticulum in maize root apices. Plant Cell Physiol. **41,** 571–582.

Sato, Y., Wada, M., and Kadota, A. (2001). Choice of tracks, microtubules and/or actin filaments, for chloroplast photo-movement is differentially controlled by phytochrome and a blue light receptor. J. Cell Sci. **114,** 269–280.

Schütze, P., Freitag, H., and Weising, K. (2003). An integrated molecular and morphological study of the subfamily Suaedoideae Ulbr. (Chenopodiaceae). Plant Syst. Evol. **239,** 257–286.

Sheahan, M.B., Rose, R.J., and McCurdy, D.W. (2004). Organelle inheritance in plant cell division: The actin cytoskeleton is required for unbiased inheritance of chloroplasts, mitochondria and endoplasmic reticulum in dividing protoplasts. Plant J. **3,** 379–390.

Sheehy, J.E., Mitchell, P.L., and Hardy, B. (2000). Redesigning Rice Photosynthesis to Increase Yield. (Makati City, Philippines: International Rice Research Institute and Elsevier Science).

Sliwinska, E., Lambert, G.M., and Galbraith, D.W. (2002). Factors affecting nuclear dynamics and green fluorescent protein targeting to the nucleus in *Arabidopsis thaliana* roots. Plant Sci. **163,** 425–430.

Staiger, C.J., and Lloyd, C.W. (1994). The plant cytoskeleton. Plant Cell Physiol. **35,** 191–204.

Van Gestel, K., Köhler, R.H., and Verbelen, J. (2002). Plant mitochondria move on F-actin, but their positioning in the cortical cytoplasm depends on both F-actin and microtubules. J. Exp. Bot. **369,** 659–667.

Voznesenskaya, E.V., Edwards, G.E., Kiirats, O., Artyusheva, E.G., and Franceschi, V.R. (2003). Development of biochemical specialization and organelle partitioning in the single celled C_4 system in leaves of *Borszczowia aralocaspica* (Chenopodiaceae). Am. J. Bot. **90,** 1669–1680.

Voznesenskaya, E.V., Franceschi, V.R., Kiirats, O., Artyusheva, E.G., Freitag, H., and Edwards, G.E. (2002). Proof of C_4 photosynthesis without Kranz anatomy in *Bienertia cycloptera* (Chenopodiaceae). Plant J. **31,** 649–662.

Voznesenskaya, E.V., Franceschi, V.R., Kiirats, O., Freitag, H., and Edwards, G.E. (2001). Kranz anatomy is not essential for terrestrial C_4 plant photosynthesis. Nature **414,** 543–546.

Voznesenskaya, E.V., Koteyeva, N.K., Chuong, S.D.X., Edwards, G.E., Akhani, H., and Franceschi, V.R. (2005). Differentiation of cellular and biochemical features of the single cell C_4 syndrome

during leaf development in *Bienertia cycloptera* (Chenopodiaceae). Am. J. Bot. **92,** 1784–1795.

Wada, M., Kagawa, T., and Sato, Y. (2003). Chloroplast movement. Annu. Rev. Plant Physiol. Plant Mol. Biol. **54,** 455–468.

Wada, M., and Suetsugu, N. (2004). Plant organelle positioning. Curr. Opin. Plant Biol. **7,** 626–631.

Wasteneys, G.O., and Galway, M.E. (2003). Remodeling the cytoskeleton for growth and form: An overview with some new views. Annu. Rev. Plant Physiol. Plant Mol. Biol. **54,** 691–722.

Wasteneys, G.O., and Yang, Z. (2004). New views on the plant cytoskeleton. Plant Physiol. **136,** 3884–3891.

Williamson, R.E. (1993). Organelle movements. Annu. Rev. Plant Physiol. Plant Mol. Biol. **44,** 181–202.

Winter, K., and Smith, J.A.C. (1996). Crassulacean Acid Metabolism. (New York: Springer).

Witztum, A., and Parthasarathy, M.V. (1985). Role of actin in chloroplast clustering and banding in leaves of *Egeria*, *Elodia* and *Hydrilla.* Eur. J. Cell Biol. **39,** 21–26.